Appl. Phys. A (2014) 116:1813–1820
DOI 10.1007/s00339-014-8334-2

Applied Physics A
Materials Science & Processing

Comparison of Cu(In, Ga)Se_2 thin films deposited on different preferred oriented Mo back contact by RF sputtering from a quaternary target

Jing Tian · Lianqin Peng · Jinwei Chen · Gang Wang · Xueqin Wang · Hong Kang · Ruilin Wang

Received: 21 November 2013 / Accepted: 17 February 2014 / Published online: 13 March 2014
© Springer-Verlag Berlin Heidelberg 2014

Abstract The Cu(In, Ga)Se_2 (CIGS) thin films were deposited on bare glass and DC sputtered preferential oriented Mo-coated glass by RF sputtering from a single quaternary target. The structural and morphological properties of the films were characterized by X-ray diffraction (XRD), Raman spectroscope, energy dispersive X-ray spectrometer (EDS) and atomic force microscope (AFM). Preferred orientation of the Mo back contact was tuned between (110) and (211) plane by controlling the thickness. All the deposited CIGS thin films show (112) preferred oriented chalcopyrite structures. The films prepared on Mo-coated glass show higher quality crystallinity, better stoichiometry composition and more smooth surface morphology. Especially, the film on (211) oriented Mo-coated glass with the best integrated performance is expected to be a candidate absorber for high-efficiency CIGS solar cell device.

1 Introduction

Chalcopyrite polycrystalline thin-film solar cells such as Cu(In, Ga)Se_2 (CIGS) compounds are important for terrestrial applications because of their high efficiency, low-cost and long-term stable performance [1–5]. High-efficiency CIGS solar cell as high as $\eta = 20.3$ % has been reported [6]. The three-stage co-evaporation process is the main method for this highest efficiency CIGS absorber in lab-scale fabrication. However, this multi-source evaporation, which consists of Cu, In, Ga, and Se as four sources, is hard to scale and achieve uniformity control on large area. Another main-stream method to fabricate CIGS absorber layers is the two-step selenization of metal precursors process, in which Cu–In–Ga metallic precursor is firstly deposited by multi-source sputtering and a post-selenization using H_2Se and Se vapor is then followed [7, 8]. However, this process has many technical drawbacks such as high selenization temperature, rough morphologies and agglomeration of Ga on the CIGS–Mo interface, etc. Thus, in recent years, several alternative "simplified" physical vapor deposition (PVD) routes, such as one-step sputtering process, "in-line" evaporation [9] and pulse electron deposition (PED) [10], have been advocated. Among them, one-step sputtering using a single quaternary target is considered as a effective way to lower the process temperature for flexible substrate and to simplify the fabrication of large-scale CIGS absorber [11–17].

Furthermore, CIGS thin films are prepared on a Mo back contact (BC) in the fabrication process of CIGS thin-film solar cells. And the past research showed that the Mo BC represented different preferred orientation with the change of layer thickness [18]. Specifically, the Mo BC's crystal growth showed a change from (110) preferred orientation to (211) preferred orientation with increasing thickness. And it is generally known that the substrate crystal orientation may affect on the thin films' crystal properties. In this study, CIGS thin films were fabricated on a series of different preferred oriented Mo-coated glasses by RF

J. Tian · L. Peng · J. Chen · G. Wang · X. Wang · H. Kang · R. Wang (✉)
College of Materials Science and Engineering, Sichuan University, Chengdu 610065, China
e-mail: rl.wang@scu.edu.cn

J. Tian
e-mail: jim_tianj@163.com

J. Tian
Education Ministry Key Laboratory of Renewable Energy Advanced Materials and Manufacturing Technology, Solar Energy Research Institute, Yunnan Normal University, Kunming 650092, China

www.spm.com.cn

Table 1 The sputtering parameters and results of the Mo BC deposited with different sputtering time

Sample	Sample-gun distance (mm)	Power (W)	Pressure (Pa)	Time (min)	Thickness (nm)	Resistivity (Ω·cm)
#1	50	60	0.78	5	172	2.280×10^{-4}
#2				10	388	1.815×10^{-4}
#3				15	562	1.553×10^{-4}
#4				20	774	1.301×10^{-4}
#5				25	948	1.068×10^{-4}

sputtering from a single chalcogenide target. Characteristics of CIGS thin films were examined by X-ray diffraction (XRD), Raman spectroscopy, atomic force microscope (AFM) and energy dispersive X-ray spectrometer (EDS).

2 Experimental

2.1 Mo back contact preparation

A DC–RF magnetron sputtering system was employed to fabricate CIGS thin film and Mo BC. The sputtering system consisted of four magnetron guns, six substrate holder, one RF generator and two DC generators. Prior to deposition, the chamber was evacuated to a background pressure of 1×10^{-4} Pa. Mo BC was deposited onto soda lime glass using a DC gun and the thicknesses were ranged from 172 to 948 nm by modifying the sputtering time between 5 and 25 min. Table 1 summarizes the Mo BC sputtering parameters and corresponding experimental results. Then, the Mo-coated soda lime glasses were ready for the subsequent CIGS thin films fabrication.

2.2 CIGS thin-film deposition

A quaternary $CuIn_{0.75}Ga_{0.25}Se_2$ chalcogenide target was used and provided by Beijing Mountain Technical Development Center for Non-ferrous metals, China. CIGS thin films were, respectively, prepared on the bare glass and previous #1, #2, #3, #4, #5 Mo-coated glasses without external heating from the quaternary target, using high-purity argon discharged with a RF power of 168 W. The working pressure was at 0.9 Pa and the target–substrate distance was about 40 mm.

2.3 Film characterization

The thicknesses of the films were measured by KLA Tencor D100 step profiler. The sheet resistances of the Mo BC were characterized using a four-point probe. The crystallographic orientation of Mo BC and CIGS thin films was determined by X-ray diffraction (Cu $K\alpha_1$ radiation, $\lambda = 1.54056$ Å, 40 kV, 25 mA). The structural properties and composition of CIGS thin films were performed by a HORIBA Jobin Yvon S.A.S LabRAM HR Raman spectroscopy with 633-nm laser and A Hitachi S4800 field emission scanning electron microscopy with an energy dispersive spectrometer. A CSPM-4000 model atomic force microscope was also employed to analyze the morphological properties of films.

3 Results and discussion

3.1 Mo back contact

Figure 1 shows that the XRD patterns of Mo back contacts deposited at various sputtering time. The Mo back contacts' crystal growth indicates a change from (110) preferred orientation to (211) preferred orientation with increasing thickness. The preferred orientation of films depends on whether it has the lowest surface energy. The thickness and resistivity of the Mo back contacts at varying sputtering times are listed in Table 1. It can be found that Mo BC thickness rises linearly with sputtering time, while the resistivity is inversed. Table 2 summarizes the XRD analysis results of the Mo BC deposited with various

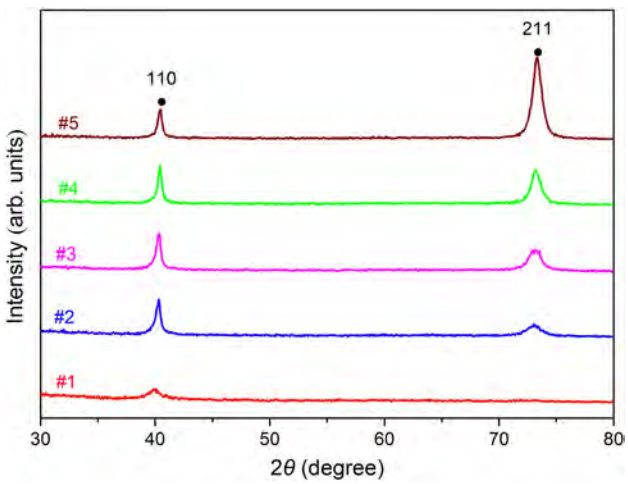

Fig. 1 XRD patterns of Mo back contacts deposited at various sputtering time

www.spm.com.cn

Table 2 The XRD analysis results of the Mo BC deposited with different sputtering time

Sample	I_{110}	I_{211}	$T_{c(211)}$	Preferred orientation
#1	176	≈0	≈0	(110)-oriented
#2	547	176	1.02	Randomly oriented
#3	537	302	1.29	(211)-oriented
#4	576	502	1.55	(211)-oriented
#5	433	1230	1.80	(211)-oriented

I_{110} intensity of Mo (110) peak, I_{211} intensity of Mo (211) peak, $T_{c(211)}$ texture coefficient of M (211) orientation

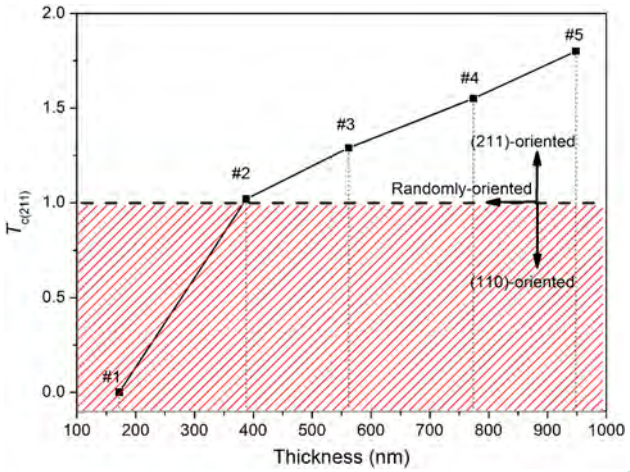

Fig. 2 The change of the preferred orientation of Mo back contacts with different thickness

sputtering time. The preferred growth of the (*hkl*) planes has been expressed in terms of the texture coefficient [19] $T_{c(hkl)}$. Quantitative information concerning the preferential crystallite orientation can been obtained from the texture coefficient, T_c, defined as:

$$T_{c(hlk)} = \frac{I_{(hkl)}/I_{r(hkl)}}{\frac{1}{n}\sum\left(I_{(hkl)}/I_{r(hkl)}\right)} \quad (1)$$

where $T_{c(hkl)}$ is the texture coefficient, $I_{(hkl)}$ are the XRD intensities obtained from the films and n is the number of diffraction peaks considered. $I_{r(hkl)}$ are the intensities of the XRD reference (JCPDS card 42-1120) to randomly oriented grains. If the value is higher than 1, the abundance of grains will aggregate in the given (*hkl*) direction. As $T_{c(hkl)}$ increases, the more preferential growth of the crystallites is shown in the perpendicular direction to the *hkl* plane. Since two diffraction peaks [(110), (211)] were considered ($n = 2$), the maximum possible value of $T_{c(211)}$ will be 2. In this case, if $0 < T_{c(211)} < 1$, (110) orientation will be preferred. Films deposited in less time with lower thickness were found to have lower $T_{c(211)}$ value. Figure 2 reveals the change of the preferred orientation of different thickness

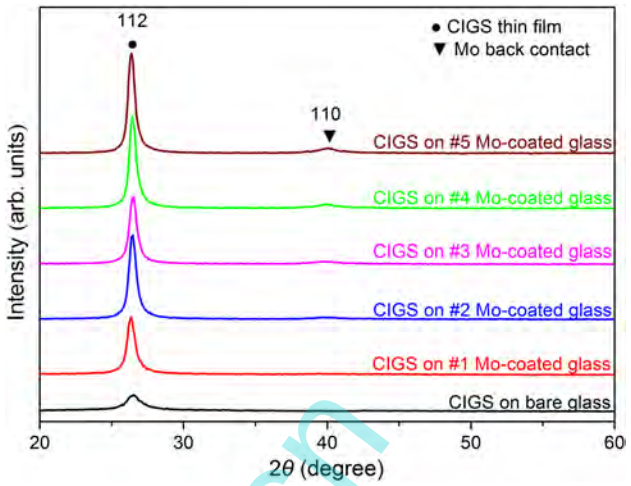

Fig. 3 XRD patterns of the CIGS thin films deposited on bare glass and different preferred oriented Mo-coated glasses

Mo back contacts. As shown in Fig. 2, #1 sample has a highest level (110) oriented, #2 sample has a randomly oriented and #5 sample has a highest level (211) oriented. It illustrates that the (110) plane of the body-centered cubic (bcc) phase has the lowest surface energy at growing early stage of Mo film. However, this circumstance is gradually replaced by (211) plane with the growth of Mo film.

3.2 CIGS thin film

Figure 3 illustrates the XRD patterns of the CIGS thin films deposited on bare glass and previous #1, #2, #3, #4 and #5 Mo-coated glass. All the films exhibit a dominant diffraction peak corresponding to CIGS (112) plane of the film. Compared with the film on bare glass, Mo-coated glass films response stronger diffraction peak intensity of the CIGS (112) plane. Notably, the two CIGS thin films deposited on #2 and #5 Mo-coated glass corresponding to the random orientation and (211) preferred orientation have much stronger diffraction peak intensity of CIGS (112) plane. This might ascribe to the grain growth of the CIGS thin films on a randomly oriented or a high level of preferred oriented Mo-coated glass. No other separate phase can be observed in the entire XRD pattern, except Mo back contact.

Figure 4 shows the XRD patterns of the CIGS powder scratched from the target and the CIGS thin films deposited on different substrates. All four samples show that the peaks can be indexed to (112), (204)/(220) and (312) characteristic peaks of the chalcopyrite-type CIGS structure (JCPDS 35-1102). The main diffraction characteristic peaks of (112) are sharp and clearly observed in all patterns. In comparison with the powder scratched from the target, all of the CIGS thin films exhibit a dominant

www.spm.com.cn

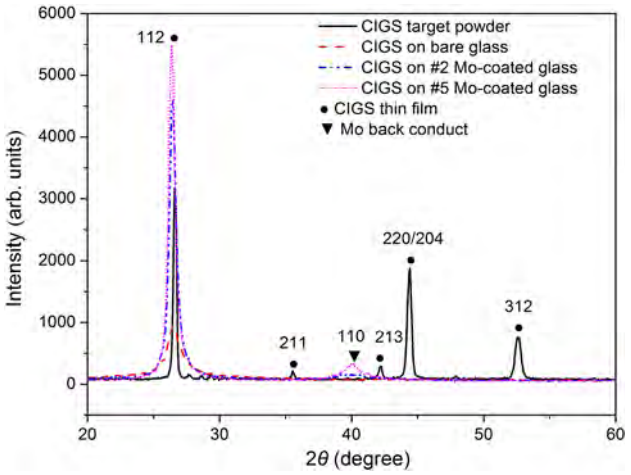

Fig. 4 XRD patterns of the CIGS target powder and thin films on different substrates

diffraction peak corresponding to CIGS (112) plane of the film and the position of (112) peak-2θ moves to a lower diffraction angle, indicating film growth preferred orientation along the (112) plane and a larger plane distance of the film. Furthermore, the latter is also due to the Cu-poor composition of the CIGS on bare glass with respect to those on Mo-coated glasses—less Cu content leads to higher 2θ angles.

Table 3 summarizes the thickness, the position of (112) peak-2θ, the intensity and the full width at half maximum value of (112) peak. With the various types of substrates from bare glass to Mo-coated glass, the intensity of CIGS (112) peak increases, and the thickness, the position of (112) peak-2θ and the full width at half maximum value of (112) peak decrease which indicate a higher crystallinity and a lower growth rate of the film. Figure 5 shows the linear fit of the sputtering rate of CIGS thin films on different types of substrate. With the sputtering time increase, the thicknesses of CIGS films on all substrates rise linearly. As shown in Fig. 5, those linear fit slopes are the sputtering rates of the films, and the intercepts illustrate that there is a non-linear process at the initial stage of film growth. The sputtering rates of CIGS films on bare, #2 Mo-coated and #5 Mo-coated glasses are 49.99, 48.69 and 26.09 nm/min, respectively. Figure 6 shows the variation of the CIGS thickness with Mo back contacts' $T_{c(211)}$. As shown in the Fig. 6, after it climbed the peak on randomly oriented Mo-coated glass, the thickness of CIGS film has declined dramatically. It might because there is a relatively low surface binding energy between Mo (211) plane and the energetic sputtering CIGS particles.

Table 3 also shows the EDS-measured chemical composition of the CIGS thin films. The films are deficient of Se and Cu element as shown in Table 3, and their content in the CIGS film on Mo-coated glass is observably higher than that in the CIGS film on bare glass. Yu et al. [17] ascribe Cu loss to the evaporation $Cu_{2-x}Se$ for its low melting point of 520 °C. It might be present in the Cu-poor plume which is sputtered out by the high-energy pulsed electron. The high temperature compensated the plume and finally resulted in the stoichiometry composition of the film. In our work, the CIGS thin films were prepared on Mo-coated glasses without external heating, so the problem of Cu loss is not too severe. In addition, Huang et al. [20] pointed out that $Cu_{2-x}Se$ secondary phase may form on the surfaces and grain boundaries in the case of polycrystalline CIGS films grown under Cu-excess condition. Our CIGS thin film on bare glass is likely to formed Cu-excess phase when the energetic sputtering CIGS particles arrive at the amorphous glass surface which has a higher surface energy than the Mo-coated glasses. The evaporation $Cu_{2-x}Se$ may explain that Cu and Se loss problem is more serious in the CIGS thin film on bare glass. Another possible explanation can be found on the phase diagram of CIGS, where an incongruent evaporation starts to appear when CIGS is heated over 1,100 °C (as it happens on the sputtered target): the vapors experience an In(Ga)-enrichment with respect to the solid phase, hence the deposited films exhibit a Cu-poor composition [21]. The Ga/(In + Ga) ratio of CIGS on Mo-coated glass has almost no deviation of stoichiometry composition compared to the designed composition ratio of the CIGS target. Theoretically [22], in 1961, Shockley and Queisser first predicted a maximum efficiency of 30.5 % for a band gap of 1.35 eV based on an illumination by black body radiation of 6,000 K. If the

Table 3 Comparative results of CIGS thin films grown on different substrates

Substrate type	Thickness (nm)	Crystalline properties by XRD			Composition by EDS		
		I_{112}	$2\theta_{112}$	FWHM	Ga/(In + Ga)	Cu/(In + Ga)	Se/(Cu + In + Ga)
Bare glass	1,363	820	26.57	1.295	0.22	0.79	0.68
#1-Mo	945	3087	26.41	0.767	\	\	\
#2-Mo	1,340	4501	26.51	0.626	0.26	0.99	0.82
#3-Mo	946	3584	26.48	0.622	\	\	\
#4-Mo	808	4926	26.45	0.618	\	\	\
#5-Mo	717	5413	26.44	0.617	0.26	0.97	0.81

I_{112} intensity of CIGS (112) peak, $2\theta_{112}$ 2θ-position of CIGS (112) peak, *FWHM* full width at half maximum value of CIGS (112) peak

www.spm.com.cn

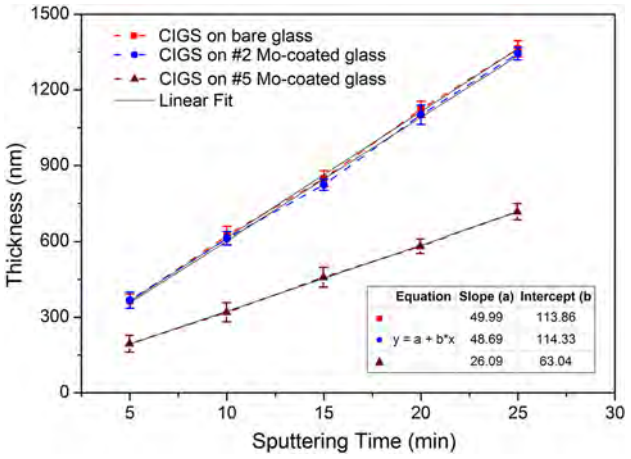

Fig. 5 Linear fit of sputtering rates of the CIGS thin films on different substrates

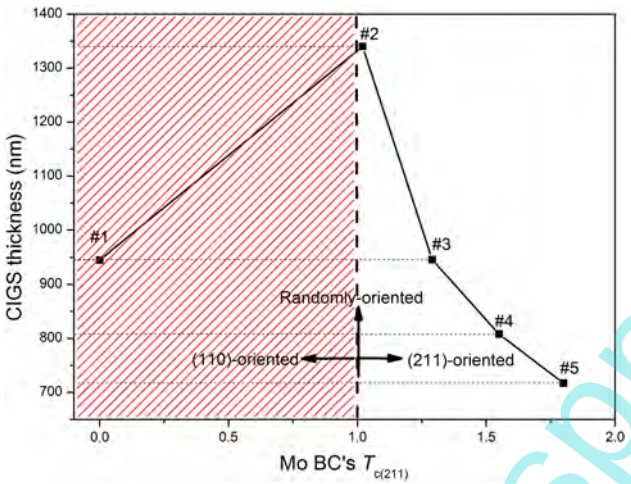

Fig. 6 The variation of the CIGS thickness with Mo back contacts' $T_{c(211)}$

efficiency is calculated in the same way but based on AM 1.5, the absorption in the solar might cause the appearance of two almost equal maxima: one of 33 % at a band gap of 1.35 eV, a second one at 32.8 % at a band gap of 1.15 eV. The latter one is very close to the band gap of observed by the low energy edge in quantum efficiency in CIGS record solar cells. As is known, the band gap of CIGS can be varied in the range of 1.04–1.72 eV by its tunable Ga/(In + Ga) ratio. U. Rau et al. [23] published an empirical calculation method to present the relationship between CIGS band gap and the Ga/(In + Ga) ratio, and the ideal ratio value range of Ga/(In + Ga) = 0.25 ~ 0.3 was given. The Ga/(In + Ga) ratios of CIGS on Mo-coated glass were in this range, but CIGS on bare glass revealed deficient of Ga element. This might be due to the re-evaporation of additional Ga element in the process of energetic particles deposited on amorphous glass surface.

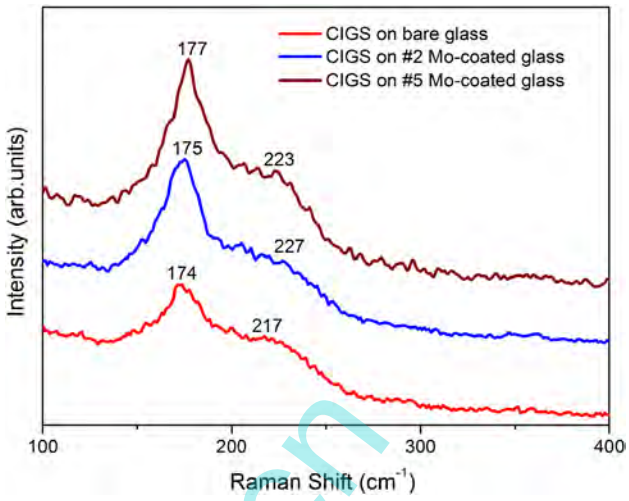

Fig. 7 Raman spectra of the CIGS thin films on different substrates

Figure 7 illustrates the Raman spectra of the films on above three kinds of glass substrates. The most intense peak within 174–177 cm^{-1} could be assigned to the A_1 mode which is the strongest mode generally observed in Raman spectra of $A^IB^{III}C_2^{VI}$ chalcopyrite compounds [24, 25]. This peak is reported to be always observed in the Raman spectra of both stoichiometric and non-stoichiometric films as long as the chalcopyrite structure of the film is not disturbed. The intensity and sharpness of the A_1 mode peak determines the composition and degree of formation of the chalcopyrite structure [11]. The frequency of the CIGS A_1 mode has a blue shift when the substrates change from Mo-coated glass to bare glass, which suggests that Cu content is reduced. In principle, this shift can be attributed to chemical variation of the quaternary alloy occurring at the surface of the films [26]. Another peak within 217–223 cm^{-1} is assigned to B_2 and E mode of the chalcopyrite CIGS, which corresponds to the combined vibration of all the atoms. It is clearly observed from Fig. 7 that the intensity and frequency of the A_1 mode increase as the substrates changes from bare glass to randomly oriented #2 Mo-coated glass to (211) oriented #5 Mo-coated glass. Roy et al. [24] pointed out that Raman spectroscopy was used to determine the film composition using the linear relation:

$$\text{Raman shift } \left(\text{cm}^{-1}\right) = 173 + 12.92x \quad (2)$$

Corresponding to the straight line joining the points 173 cm^{-1} for $CuInSe_2$ and 186 cm^{-1} for $CuGaSe_2$. It illustrates that the x = Ga/(In + Ga) values increase with the change of substrates. These chemical composition results are also consistent with the above mentioned EDS test. Meanwhile, they considered that, in the relation (2), it is inherent assumption that only indium atom is replaced by Gallium for higher x values in CIGS and the remaining atoms in the lattice are intact. But this is not always

www.spm.com.cn

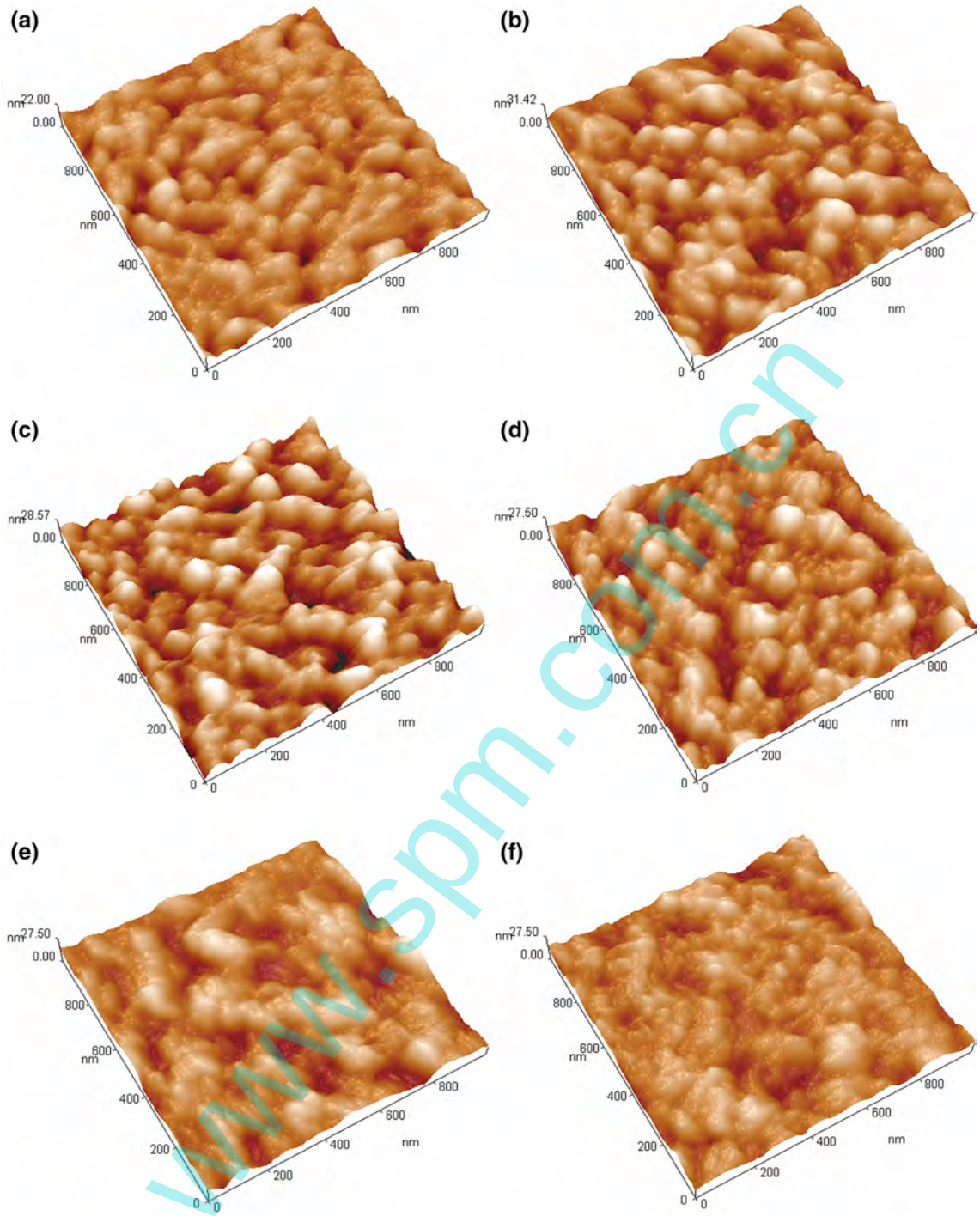

Fig. 8 AFM images of CIGS thin films deposited on **a** bare glass and **b–f** #1–#5 Mo-coated glasses

obtained in practice and there are also some changes in the lattice due to slight variation from stoichiometry. This may explain the deviation between calculation results and EDS data [27]. To clarify the effects of changing substrates further, the full width at half maximum (FWHM) values of A_1 mode peaks can be employed. The FWHM values of the CIGS thin films on bare, #2 Mo-coated and #5 Mo-coated glass are 107, 81 and 79 cm^{-1}, respectively. The Mo-coated glass substrates significantly reduced the FWHM values while raised the degree of single-phase chalcopyrite structure. This is identical to the previous XRD discussion. In addition, an increase of FWHM value also indicates the reduction of Cu content. FWHM broadening is interpreted as a result of a higher density of defects within the CIGS

www.spm.com.cn

Table 4 Comparative AFM results of CIGS thin films deposited on bare and different preferred oriented Mo-coated glass

Substrate type	R_a (nm)	RMS (nm)	D_p (nm)
Bare glass	1.76	2.28	47.7
#1 Mo	3.73	4.63	52.7
#2 Mo	4.31	5.41	63.3
#3 Mo	3.16	3.96	66.4
#4 Mo	2.75	3.47	232.4
#5 Mo	2.18	2.77	243.6

R_a roughness average, *RMS* roughness root mean square value, D_p surface mean particle diameter and the bold sample were chosen to represent previous comparison of CIGS films on different substrates

chalcopyrite phase for films with lower Cu content, for which the formation of Cu vacancies—ordered vacancy compound (OVC) phase becomes more likely. But in the spectra, the peak attributed to OVC did not appear at around 152 cm^{-1} for all samples [27], which is preferable.

Figure 8 shows the AFM images of CIGS thin films deposited on bare and different preferred oriented Mo-coated glass, and Table 4 summarizes corresponding analytical data. Overall, the morphology reveals a transformation from particle to cluster with increasing value of Mo $T_{c(211)}$. Specifically, as shown in Fig. 8a, surface of the film deposited on bare glass is distributed with particles approximately 47.7 nm in mean diameter (D_p). The particles have no clear crystalline face and edges but continuous irregular hollows. The roughness average (R_a) and root mean square (RMS) are 1.76 and 2.28 nm, respectively. It illustrates the morphology of film with a smooth surface. Deposition of the chalcopyrite CIGS thin films with a smooth surface is essential for fabricating a high-quality solar cell device [11]. The crystal structure of the films deposited on Mo-coated glass was considerably improved, forming well-defined crystal grain as demonstrated in Fig. 8b–f. The surface of CIGS thin film deposited on randomly oriented #2 Mo-coated glass, as shown in Fig. 8c, is covered with clear faceted CIGS particles with $D_p = 63.3$ nm, $R_a = 4.31$ nm and RMS = 5.41 nm, respectively. Meanwhile, the surface of CIGS thin film deposited on (211) oriented #5 Mo-coated glass, as shown in Fig. 8f, is uniformly distributed with clusters consisting of several particles with $D_p = 243.6$ nm. This dramatical increase of grain dimension may explain that the sample has higher (112) peak intensity in XRD test. The irregular hollows become shallow and the roughness dramatically reduces to $R_a = 2.18$ nm and RMS = 2.77 nm.

4 Conclusions

This study reports the characteristics of CIGS thin films deposited on bare glass and different preferred oriented Mo-coated glass by RF sputtering from a single target. The Mo BC's crystal growth has a change from (110) to (211) plane preferred orientation with increasing thickness, which was employed to prepare different preferred oriented Mo-coated glass substrates for the deposition of CIGS thin films. All the deposited CIGS thin films reveal (112) plane preferred oriented chalcopyrite structures. The films prepared on Mo-coated glass show higher quality crystallinity, better stoichiometry composition and more smooth surface morphology. Especially, the film on (211) oriented #5 Mo-coated glass with a higher $T_{c(211)} = 1.80$ exhibits the best integrated performance to satisfy the needs of high-efficiency CIGS solar cell device while it has the lowest growth rate when compared with others.

Acknowledgments This work is supported by the National Scientific Foundation of China (NSFC project No. 21306119), Specialized Research Fund for the Doctoral Program of Higher Education (No. 20110181110003), Collaborative innovation fund by China Academy of Engineering Physics and Sichuan University (No. XTCX2011001), the Provincial Natural Science Foundation of Sichuan (No. 2013FZ0034, No. 2013JY0150), the financial support by China Academy of Engineering Physics under contract (No. HG2012039) and Yunnan Education Department Scientific Research Fund (Grant No. 2012Y170).

References

1. S. Niki, M. Contreras, I. Repins, M. Powalla, K. Kushiya, S. Ishizuka, K. Matsubara, Prog. Photovoltaics Res. Appl. **18**, 453–466 (2010)
2. M. Acciarri, S. Binetti, A. Le Donne, B. Lorenzi, L. Caccamo, L. Miglio, R. Moneta, S. Marchionna, M. Meschia, Cryst. Res. Technol. **46**, 871–876 (2011)
3. M. Gu, X.Q. Zhang, X.D. Xiao, Proc. of SPIE-OSA-IEEE **8312**, 83120H (2011)
4. I. Repins, M.A. Contreras, B. Egaas, C. DeHart, J. Scharf, C.L. Perkins, B. To, R. Noufi, Prog. Photovoltaics Res. Appl. **16**, 235–239 (2008)
5. M.A. Green, K. Emery, Y. Hishikawa, W. Warta, E.D. Dunlop, Prog. Photovoltaics Res. Appl. **21**, 1–11 (2013)
6. P. Jackson, D. Hariskos, E. Lotter, S. Paetel, R. Wuerz, R. Menner, W. Wischmann, M. Powalla, Prog. Photovoltaics Res. Appl. **19**, 894–897 (2011)
7. N.M. Park, H.S. Lee, D.H. Cho, Y.D. Chung, K.H. Kim, K.S. Lee, J. Kim, Prog. Photovoltaics. Res. Appl. **20**, 899–903 (2012)
8. N.G. Dhere, V.S. Gade, A.H. Jahagirdar, A.A. Kadam, H.P. Patil, S.S. Kulkarni, J. Vac. Sci. Thechnol. A. **21**, 1442 (2003)
9. J. Lindahl, J.T. Wätjen, A. Hultqvist, T. Ericson, M. Edoff, T. Törndahl, Prog. Photovoltaics Res. Appl. **21**, 1588–1597 (2013)
10. S. Rampino, N. Armani, F. Bissoli, M. Bronzoni, D. Calestani, M. Calicchio, N. Delmonte, E. Gilioli, E. Gombia, R. Mosca, L. Nasi, F. Pattini, A. Zappettini, M. Mazzer, Appl. Phys. Lett. **101**, 132107 (2012)
11. J.H. Shi, Z.Q. Li, D.W. Zhang, Q.Q. Liu, Z. Sun, S.M. Huang, Prog. Photovoltaics Res. Appl. **19**, 160–164 (2011)
12. Y.C. Lin, J.H. Ke, W.T. Yen, S.C. Liang, C.H. Wu, C.T. Chiang, Appl. Surf. Sci. **257**, 4278–4284 (2011)
13. C.H. Chen, T.Y. Lin, C.H. Hsu, S.Y. Wei, C.H. Lai, Thin Solid Films **535**, 122–126 (2013)

www.spm.com.cn

14. T.W. Kim, Y.B. Kim, S.I. Song, C.W. Jung, J.H. Lee, Proc. of SPIE **8110**, 811008 (2011)
15. J. Liu, D.M. Zhuang, H.X. Luan, M.J. Cao, M. Xie, X.L. Li, Prog. Nat. Sci. Mater. Int. **23**, 133–138 (2013)
16. S.J. Pak, J.H. Kim, Curr. Appl. Phys. **13**, 1046–1049 (2013)
17. Z. Yu, Y. Yan, S. Li, Y.X. Zhang, C.P. Yan, L. Liu, Y. Zhang, Y. Zhao, Appl. Surf. Sci. **264**, 197–201 (2013)
18. J. Tian, X. Yang, S.J. Liu, X.J. Lian, J.W. Chen, R.L. Wang, Acta Phys. Sin. **62**, 116801 (2013)
19. R. Romero, D. Leinen, E.A. Dalchiele, J.R. Ramos-Barrado, F. Martín, Thin Solid Films **515**, 1942–1949 (2006)
20. X. Huang, X.S. Miao, N.N. Yu, X.W. Guan, Appl. Surf. Sci. **287**, 257–262 (2013)
21. S. Rampino, F. Bissoli, E. Gilioli, F. Pattini, Prog. Photovoltaics Res. Appl. **21**, 588–594 (2011)
22. S. Siebentritt, Sol. Energy Mater. Sol. Cells **95**, 1471–1476 (2011)
23. U. Rau, M. Schmidt, A. Jasenek, G. Hanna, H.W. Schock, Sol. Energy Mater. Sol. Cells **67**, 137–143 (2011)
24. S. Roy, P. Guha, S.N. Kundu, H. Hanzawa, S. Chaudhuri, A.K. Pal, Mater. Chem. Phys. **73**, 24–30 (2002)
25. W. Liu, Y. Sun, W. Li, C.J. Li, F.Y. Li, J.G. Tian, Appl. Phys. A Mater. **88**, 653–656 (2007)
26. R. Caballero, V. Izquierdo-Roca, X. Fontané, C.A. Kaufmann, J. Álvarez-García, A. Eicke, L. Calvo-Barrio, A. Pérez-Rodríguez, H.W. Schock, J.R. Morante, Acta Mater. **58**, 3468–3476 (2010)
27. Yunae Cho, Dong-Wook Kim, SeJin Ahn, Dahyun Nam, Hye-onsik Cheong, Guk Yeong Jeong, Jihye Gwak, Jae Ho Yun, Thin Solid Films **546**, 358–361 (2013)

www.spm.com.cn